




Article

# Constraints on Barrow Entropy from M87\* and S2 Star Observations

Kimet Jusufi <sup>1</sup>, Mustapha Azreg-Ainou <sup>2</sup>, Mubasher Jamil <sup>3,4</sup> and Emmanuel N. Saridakis <sup>5,6,\*</sup>

<sup>1</sup> Physics Department, State University of Tetovo, Ilinden Street nn, 1200 Tetovo, North Macedonia; kimet.jusufi@unite.edu.mk

<sup>2</sup> Engineering Faculty, Başkent University, Bağlıca Campus, Ankara 06790, Turkey; azreg@baskent.edu.tr

<sup>3</sup> Institute for Theoretical Physics and Cosmology, Zhejiang University of Technology, Hangzhou 310023, China; mjamil@zjut.edu.cn

<sup>4</sup> School of Natural Sciences, National University of Sciences and Technology, Islamabad 44000, Pakistan

<sup>5</sup> National Observatory of Athens, Lofos Nymfon, 11852 Athens, Greece

<sup>6</sup> CAS Key Laboratory for Researches in Galaxies and Cosmology, Department of Astronomy, University of Science and Technology of China, Hefei 230026, China

\* Correspondence: msaridak@phys.uoa.gr

**Abstract:** We use data from M87\* central black hole shadow, as well as from the S2 star observations, in order to extract constraints on Barrow entropy. The latter is a modified entropy arising from quantum-gravitational effects on the black hole horizon, quantified by the new parameter  $\Delta$ . Such a change in entropy leads to a change in temperature, as well as to the properties of the black hole and its shadow. We investigate the photon sphere and the shadow of a black hole with Barrow entropy, and assuming a simple model for infalling and radiating gas we estimate the corresponding intensity. Furthermore, we use the radius in order to extract the real part of the quasinormal modes, and for completeness we investigate the spherical accretion of matter onto the black hole, focusing on isothermal and polytropic test fluids. We extract the allowed parameter region, and by applying a Monte-Carlo-Markov Chains analysis we find that  $\Delta \simeq 0.0036_{-0.0145}^{+0.0792}$ . Hence, our results place the upper bound  $\Delta \lesssim 0.0828$  at  $1\sigma$ , a constraint that is less strong than the Big Bang Nucleosynthesis one, but significantly stronger than the late-time cosmological constraints.

**Keywords:** modified gravity; barrow entropy; black holes shadow



**Citation:** Jusufi, K.; Azreg-Ainou, M.; Jamil, M.; Saridakis, E.N. Constraints on Barrow Entropy from M87\* and S2 Star Observations. *Universe* **2022**, *8*, 102. <https://doi.org/10.3390/universe8020102>

Academic Editors: Noemi Frusciante, Francesco Pace and Gonzalo J. Olmo

Received: 22 October 2021

Accepted: 25 January 2022

Published: 4 February 2022

**Publisher's Note:** MDPI stays neutral with regard to jurisdictional claims in published maps and institutional affiliations.



**Copyright:** © 2022 by the authors. Licensee MDPI, Basel, Switzerland. This article is an open access article distributed under the terms and conditions of the Creative Commons Attribution (CC BY) license (<https://creativecommons.org/licenses/by/4.0/>).

## 1. Introduction

Black holes are currently the leading astrophysical laboratories for testing general relativity as well as theories of modified and quantum gravity. In particular, recent advances in optical, radio, X-ray and gravitational wave astronomy [1–3] have confirmed the presence of supermassive black holes in the galactic centers of giant elliptical and spiral galaxies, as well as small astrophysical black holes. Due to the observation of the first radio images of the supermassive black hole that exists at the center of the M87\* galaxy, by Event Horizon Telescope (EHT), black-hole shadows have become a very useful tool to test general relativity and examine whether possible deviations due to gravitational modifications [4,5] could indeed be the case. In such researches, one first calculates the shadows of various black hole solutions [6–37] and then confronts them with the M87\* data [38–65].

On the other hand, one of the most intriguing discoveries is the theoretical connection between thermodynamics and gravity, which may play a significant role to understand more deeply the nature of black holes. In the classical relativistic picture, black holes can decrease the entropy of the universe by swallowing objects and therefore violating the second law of thermodynamics. To resolve this problem, Bekenstein [66] conjectured that black holes should have entropy. This idea was shown by Hawking using the semi-classical approach to be correct, and it was found that black holes radiate away energy

and consequently the external observer would associate a temperature to the black hole horizon [67]. The laws of black hole thermodynamics relate the horizon temperature with the surface gravity. Hence, the black hole entropy, namely the Bekenstein-Hawking entropy, is given by  $S_B = A/4$ , where  $S_B$  is the entropy and  $A$  the surface area of the black hole (in units where  $\hbar = G = c = 1$ ).

Recently, Barrow argued that quantum-gravitational effects induce a fractal structure on the black hole horizon, which then acquires spatial dimension more than two but less than three, quantified by the parameter  $\Delta$  [68]. Hence, such a complex structure leads to a modification of the black hole entropy. This idea may have interesting consequences in cosmological and holographic applications [69–80]. Nevertheless, it also has interesting implications on the black hole properties itself, since it changes the black hole temperature too [81–83].

In this work we are interested in extracting constraints on the Barrow exponent  $\Delta$ , using data from the M87\* central black hole shadow, as well as from the S2 star observations. The manuscript is organized as follows. In Section 2, we review Barrow entropy. In Section 3 we apply the involved expressions in order to find the black hole properties and the shadow images. Moreover, in Section 4 we use the M87\* observations and we analyze the motion of the S2 star orbit to fit the data and improve the constraints on the Barrow parameter. Finally, in Section 5 we conclude. For completeness, in the Appendix A, we consider the spherical accretion of isothermal and polytropic fluids onto black holes with Barrow entropy.

## 2. Black Holes with Barrow Entropy

Barrow proposed a modification of Bekenstein-Hawking black hole entropy induced by quantum gravity effects on its horizon [68]. The corresponding corrections change the exponent of the entropy-area law, leading to

$$S_B = \left(\frac{A}{4}\right)^{1+\frac{\Delta}{2}}, \tag{1}$$

where  $\Delta$  is the new parameter, and with  $A$  the usual area of the black hole’s event horizon.  $\Delta$  is restricted to the interval  $0 \leq \Delta \leq 1$ , with  $\Delta = 0$  giving the standard Bekenstein–Hawking entropy, while  $\Delta = 1$  corresponding to the maximal deformation of the horizon structure.

In this work we will focus on Schwarzschild black hole solutions, with metric

$$ds^2 = -f(r)dt^2 + \frac{dr^2}{f(r)} + r^2(d\theta^2 + \sin^2\theta d\phi^2). \tag{2}$$

If the mass parameter is  $M$ , the corresponding horizon is  $r_H = 2M$ , and as usual we can express its area as  $A = 4\pi r_H^2 = 16\pi M^2$ . In this case (1) can be re-written as  $S_B(M) = (4\pi M^2)^{1+\frac{\Delta}{2}}$ . Hence, using that  $\frac{1}{T} = \frac{\partial S_B}{\partial M}$ , one can find the modified black hole temperature [84] arising from the modified Barrow entropy as [81].

$$T_B = \frac{1}{(\Delta + 2)(4\pi)^{1+\frac{\Delta}{2}} M^{1+\Delta}}. \tag{3}$$

In summary, the effect of Barrow entropy is to change the black hole temperature too, while in the case  $\Delta = 0$  we re-obtain the standard Hawking temperature  $T = 1/(8\pi M)$ .

Let us proceed by considering a standard Schwarzschild black hole solution that would have the same temperature with the above Barrow temperature. Using the well-known expression for the black hole temperature  $T = \frac{f'(r)}{4\pi} |_{r=\tilde{r}_H}$ , with  $\tilde{r}_H$  the horizon, we can easily see that in this case the corresponding metric function should be

$$f(r) = 1 - \frac{(\Delta + 2)M^{\Delta+1}(4\pi)^{\frac{\Delta}{2}}}{r}, \tag{4}$$

and thus the horizon should be

$$\tilde{r}_H = (4\pi)^{\frac{\Delta}{2}} (\Delta + 2) M^{\Delta+1}, \tag{5}$$

and the mass

$$\tilde{M} = (4\pi)^{\frac{\Delta}{2}} \left(\frac{\Delta}{2} + 1\right) M^{\Delta+1}. \tag{6}$$

In the limiting case where Barrow entropy becomes standard Bekenstein-Hawking entropy, i.e., for  $\Delta = 0$ , the above solution becomes the standard one.

Now, it is well known that the Hawking temperature can be also understood geometrically by Wick-rotating the time coordinate  $t \rightarrow i\tau$  and  $r \rightarrow \tilde{r}_H + \delta r$ . Thus,

$$f(r) = \frac{r - \tilde{r}_H}{r}, \tag{7}$$

and then near the horizon we have  $f(r) \simeq f'(r)|_{\tilde{r}_H}(r - \tilde{r}_H)$ , and the metric (2) reads [84].

$$ds^2 = \frac{\delta r^2}{\tilde{r}_H} d\tau^2 + \frac{\tilde{r}_H}{\delta r} d(\delta r)^2 + \tilde{r}_H^2 (d\theta^2 + \sin^2 \theta d\phi^2). \tag{8}$$

Defining a new radial coordinate  $\rho$  as  $\rho = 2\sqrt{\tilde{r}_H \delta r}$ , the line element acquires the form

$$ds^2 \simeq \frac{\rho^2}{4\tilde{r}_H^2} d\tau^2 + d\rho^2 + \tilde{r}_H^2 (d\theta^2 + \sin^2 \theta d\phi^2). \tag{9}$$

In order to avoid the conical singularity we can impose the periodicity of the Euclidean time coordinate  $\tau$  as

$$\frac{\tau}{2\tilde{r}_H} \sim \frac{\tau}{2\tilde{r}_H} + 2\pi, \tag{10}$$

and then we can identify the inverse of the period of the Euclidean time coordinate to correspond to the temperature [84]. In particular, in the Euclidean path integral formulation we can make the identification for the finite temperature field theory using the relation.

$$\int [D\phi] e^{\int_0^{t_0} dt L(\phi)} = \text{Tr}(e^{-t_0 H}) = \text{Tr}(e^{-\frac{H}{T}}), \tag{11}$$

which holds for any field  $\phi$ , with which one finds that the Schwarzschild black hole (2) has temperature  $T = 1/(4\pi\tilde{r}_H)$ , which using (5) gives exactly a Hawking temperature that coincides with (3).

### 3. Barrow Entropy Effect on Black Hole Shadows

In this section we use the Schwarzschild-like metric which we found by using the Barrow corrected black hole temperature in order to study the shadow of a black hole possessing Barrow entropy. As it is known, there are two constants of motion for particle motion in spherically symmetric geometry, due to the existence of the timelike and spacelike Killing vectors, namely the energy  $E$  and the angular momentum  $L$  of the particle, in our case photon, respectively. Following the standard procedure it is straightforward to obtain the equations of motion for the photon [12].

$$\frac{dt}{d\lambda} = \frac{E}{f(r)}, \tag{12}$$

$$\frac{dr}{d\lambda} = \frac{\sqrt{R(r)}}{r^2}, \tag{13}$$

$$\frac{d\theta}{d\lambda} = \frac{\sqrt{\Theta(\theta)}}{r^2}, \tag{14}$$

$$\frac{d\phi}{d\lambda} = \frac{L \csc^2 \theta}{r^2}, \tag{15}$$

where

$$R(r) \equiv E^2 r^4 - (\mathcal{K} + L^2) r^2 f(r), \tag{16}$$

$$\Theta(\theta) \equiv \mathcal{K} - L^2 \csc^2 \theta \cos^2 \theta, \tag{17}$$

where  $\mathcal{K}$  is a constant of integration known as the Cartan constant. It simply follows from the separation of the Hamilton-Jacobi equations into a radial part and a polar part setting each part equal to  $\mathcal{K}$  [85]. Using the above equations we can further study the radial geodesics by introducing the effective potential  $V_{\text{eff}}(r)$  as follows

$$\left(\frac{dr}{d\lambda}\right)^2 + V_{\text{eff}}(r) = 0, \tag{18}$$

where

$$V_{\text{eff}}(r) = -1 + \frac{f(r)}{r^2} (\xi^2 + \eta), \tag{19}$$

and

$$\xi = \frac{L}{E}, \quad \eta = \frac{\mathcal{K}}{E^2}. \tag{20}$$

We can use the two parameters  $\xi$  and  $\eta$  in order to analyze the motion of photons around the black hole. Since we are interested to explore the effect of the Barrow parameter on the shadow of the black hole, we need to use the conditions for unstable orbit. As we know, in the observer’s sky, we can observe the black hole shadow due to the fact that some of the scattered photons escape from the black hole and some of the photons are captured by the black hole geometry. In other words, the black hole shadow is obtained as a union of the dark spots in the observer’s sky. While it is straightforward to see that the critical orbits are characterized by certain critical values in terms of the impact parameters  $\xi$  and  $\eta$ . To determine the critical orbits or the unstable circular photon orbits, we simply need to study the effective potential, that is we need to find the maximum of the effective potential  $V_{\text{eff}}$  yielding the unstable orbits. Thees unstable circular photon orbits can be obtained by applying the following conditions:

$$V_{\text{eff}} = 0, \quad V'_{\text{eff}}(r) = 0, \quad V''_{\text{eff}}(r) \leq 0.$$

Using Equations (13) and (18) it is easy to combine  $V_{\text{eff}}$  and  $R(r)$ . If we express the above conditions in terms of  $R(r)$  we obtain:

$$R(r) = 0, \quad \frac{dR(r)}{dr} = 0, \quad \frac{d^2R(r)}{dr^2} > 0. \tag{21}$$

In terms of the above conditions one can easily show that the photon radius is determined by the following algebraic condition

$$2f(r) - rf'(r) = 0. \tag{22}$$

By solving (22) under (4), we obtain a simple relation for the radius of the photon sphere  $r_{\text{ph}}$  given by

$$r_{\text{ph}} = \frac{3}{2}(2 + \Delta)M^{\Delta+1}(4\pi)^{\frac{\Delta}{2}} = \frac{3}{2}\tilde{r}_H. \tag{23}$$

The radius of the photon sphere can be used to find the size of black hole shadow. In order to describe the shadow as seen by large distances, one introduces the two celestial coordinates  $X$  and  $Y$  [85], namely  $X = \lim_{r_* \rightarrow \infty} (-r_*^2 \sin \theta_0 \frac{d\phi}{dr})$  and  $Y = \lim_{r_* \rightarrow \infty} r_*^2 \frac{d\theta}{dr}$ , with  $r_*$  the distance between the black hole and the observer, and  $\theta_0$  the inclination angle

between the observer’s line of sight and the black hole rotational axis. Using the geodesics equations we finally obtain [86].

$$X = -\xi(r_{\text{ph}}) \csc \theta_0, \tag{24}$$

$$Y = \sqrt{\eta(r_{\text{ph}}) - \xi^2(r_{\text{ph}}) \cot^2 \theta_0}, \tag{25}$$

and thus we have  $X^2 + Y^2 = \xi^2(r_{\text{ph}}) + \eta(r_{\text{ph}})$ . Hence, the event horizon (i.e., shadow) radius  $R_{\text{sh}}$  can finally be found as [12].

$$R_{\text{sh}}(r_{\text{ph}}) = \sqrt{\xi^2(r_{\text{ph}}) + \eta(r_{\text{ph}})} = \frac{r_{\text{ph}}}{\sqrt{f(r_{\text{ph}})}}, \tag{26}$$

which explicitly yields

$$R_{\text{sh}} = 3\sqrt{3}(\Delta + 2)2^{\Delta-1}M^{\Delta+1}(4\pi)^{\frac{\Delta}{2}}. \tag{27}$$

We can see that the event horizon radius is expected to increase due to the effect of quantum gravity corrections, since  $M > 0$  and  $\Delta \geq 0$ .

We continue by using the inverse relationship between  $R_{\text{sh}}$  and the real part of quasinormal modes given by [87,88].

$$\omega_{\Re} = \lim_{l \gg 1} \frac{l + \frac{1}{2}}{R_{\text{sh}}}, \tag{28}$$

with  $l$  the multipole numbers, which in our case gives

$$\omega_{\Re} = \lim_{l \gg 1} \frac{l + \frac{1}{2}}{3\sqrt{3}(\Delta + 2)2^{\Delta-1}M^{\Delta+1}(4\pi)^{\frac{\Delta}{2}}}. \tag{29}$$

In Table 1 we present the numerical values for the photon radius, the values for the shadow radius, and the real part of quasinormal modes by varying the Barrow parameter. One can see that while the shadow radius increases by increasing  $\Delta$ , the value of  $\omega_{\Re}$  decreases. As we already mentioned, relation (29) is precise in the eikonal limit, namely  $l \rightarrow \infty$ , however it has been shown that in many cases it gives satisfactory results even for small  $l$ , which are most important for observations [87,88]. Finally, the decrease in  $\omega_{\Re}$  is therefore simply explained from the inverse relation between the real part of the quasinormal modes and the shadow radius, according to (28).

**Table 1.** The photon sphere radius  $r_{\text{ph}}$ , the event horizon radius  $R_{\text{sh}}$  and the real part of quasinormal modes  $\omega_{\Re}$ , for different values of  $\Delta$ , with  $M = 1$  and  $l = 1$ .

$\Delta$	$r_{\text{ph}}$	$R_{\text{sh}}$	$\omega_{\Re}$
0	3	5.196152424	0.5000000000
0.001	3.005300838	5.205333745	0.4991180853
0.005	3.026590476	5.242208479	0.4956071896
0.008	3.042648663	5.270022075	0.4929915236
0.010	3.053397641	5.288639851	0.4912560290
0.030	3.162827055	5.478177156	0.4742592542
0.050	3.275860255	5.673956398	0.4578949904
0.080	3.452414952	5.979758107	0.4344784798
0.100	3.574958849	6.192010363	0.4195852494
0.120	3.701516690	6.411214974	0.4052392912
0.150	3.899154632	6.753533931	0.3846987723
0.170	4.036303659	6.991083014	0.3716271436
0.200	4.250450140	7.361995599	0.3529037985

We close this section by considering the scenario where the black hole is surrounded by an infalling/radiating accretion flow. Via this simple model, we can extract valuable information about the intensity of the radiation which can be detected by a distant observer. In order to achieve this we need to estimate the specific intensity at the observed photon frequency  $\nu_{obs}$  at the point  $(X, Y)$  of the observer’s image [37,47,89–92].

$$I_{obs}(\nu_{obs}, X, Y) = \int_{\gamma} g^3 j(\nu_e) dl_{prop}. \tag{30}$$

The freely falling gas has the four-velocity components written as

$$u_e^\mu = \left( \frac{1}{f(r)}, -\sqrt{1 - f(r)}, 0, 0 \right), \tag{31}$$

with  $f(r)$  given in (4). In addition we need to use the condition  $p_\mu p^\mu = 0$ , from which one can easily show that

$$\frac{p^r}{p^t} = \pm f(r) \sqrt{f(r) \left( \frac{1}{f(r)} - \frac{b^2}{r^2} \right)}, \tag{32}$$

with  $b$  the impact parameter. It is important to mention here that sign  $+(-)$  describes the case when the photon approaches (or draws away) from the black hole. The redshift function  $g$  can be calculated using [37,47,89–92].

$$g = \frac{p_\mu u_{obs}^\mu}{p_\nu u_e^\nu}, \tag{33}$$

with  $u_{obs}^\mu$  the 4-velocity of the observer. For the specific emissivity we assume a simple model in which the emission is monochromatic, with emitter’s-rest frame frequency  $\nu_*$ , and the emission has a  $1/r^2$  radial profile:

$$j(\nu_e) \propto \frac{\delta(\nu_e - \nu_*)}{r^2}, \tag{34}$$

where  $\delta$  denotes the Dirac delta function. Expressing the proper length in terms of radial coordinate for observed flux, we find

$$F_{obs}(X, Y) \propto - \int_{\gamma} \frac{g^3 p_t}{r^2 p^r} dr. \tag{35}$$

In order to show all the above in a more transparent way, in Figure 1 we present the black hole shadow for fixed  $M$  and various values of Barrow exponent  $\Delta$ , according to (27). Additionally, we have numerically calculated and depicted the intensity from (35). As we observe, with increasing Barrow parameter the size of the shadow increases, while the intensity decreases.

Lastly, since we have extracted the black hole profile and properties we can straightforwardly investigate the accretion of matter onto it. For completeness, we provide this analysis in the Appendix A.

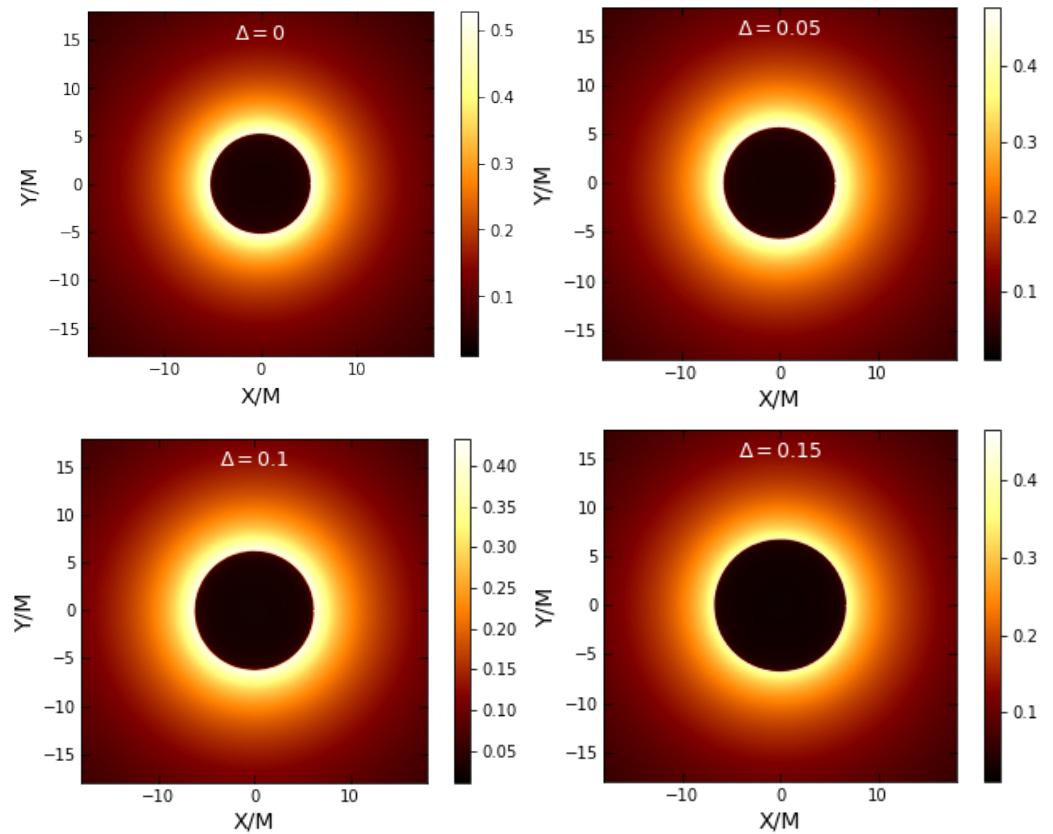


**Figure 1.** The shadow images and intensities for various values of Barrow exponent  $\Delta$ , for fixed  $M = 1$ .

#### 4. Observational Constraints on the Barrow Parameter

In this section we proceed to the use of the Event Horizon Telescope observations for the shadow of the M87\* central black hole in order to impose constraints on the Barrow parameter  $\Delta$ . As we will see, this will not be adequate and thus we need to incorporate additional data from the S2 star orbit observations [93,94].

The M87\* central black hole has angular diameter  $\theta_{sh} = (42 \pm 3)\mu as$ , is at distance  $D = 16.8$  Mpc, and its mass is  $(6.5 \pm 0.9) \times 10^9 M_{\odot}$ . We equate this to  $\bar{M}$  given in (6) in terms of the parameters  $\Delta$  and  $M$ . Thus, we treat  $M$  as a parameter and not the true mass of the system. From a theoretical point of view this can be advantageous, since spherical solutions may be modeled differently, where each theoretical model introduces a set of parameters that have to be constrained to fit observational data. In this work we model M87\* as a Barrow quantum-corrected two-parameter black hole, while one could model it using alternative theories of gravity too (see e.g., [95,96]).

Combining the observational parameters allows us to introduce the single quantity  $d_{M87*}$ , which accounts for the size of the M87\*'s shadow in unit mass, as [48].

$$d_{M87} = \frac{D \theta_{sh}}{M_{87}} = 11.0 \pm 1.5. \tag{36}$$

In particular within  $1\sigma$  confidence level one has the range  $9.5 \leq d_{M87} \leq 12.5$ .

Let us now use the theoretically predicted shadows of the previous section, in order to calculate the predicted diameter per unit mass  $d_{sh}$  for black holes with Barrow entropy. In Figure 2 we depict  $d_{sh}$  as a function of  $\Delta$ , for fixed  $M = 1$ , alongside the observational bounds according to (36).

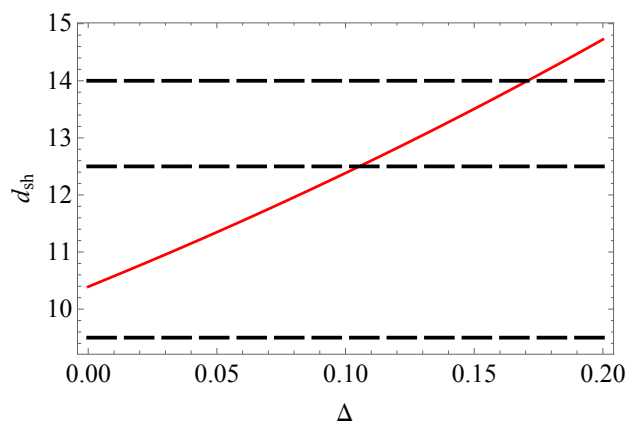


**Figure 2.** The theoretically predicted diameter per unit mass  $d_{sh}$ , for black holes with Barrow entropy, as a function of  $\Delta$  and for fixed  $M = 1$ . The horizontal dashed lines at 9.5 and 12.5 mark the  $1\sigma$  bounds according to  $d_{M87^*}$  observations, given in (36), while the horizontal dashed line at 14 marks the upper  $2\sigma$  bound (the lower  $2\sigma$  bound is not shown since it corresponds to the not physically interested region  $\Delta < 0$ ).

Nevertheless, as one can see, in general the results depend on both  $\Delta$  and  $M$ . Indeed, in Figure 3 we present the parameter region which is consistent with M87\* data.

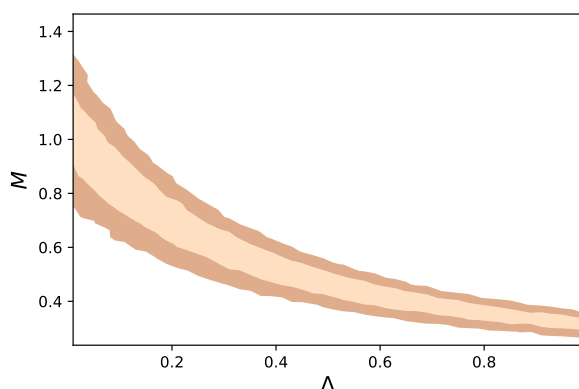


**Figure 3.**  $1\sigma$  and  $2\sigma$  parameter region consistent with M87\* shadow observations.

Additionally, in Figure 4 we present the predicted combined diameter  $d_{sh}$  as a function of  $M$  and  $\Delta$ .

In order to break the degeneracy, and constrain  $\Delta$  more efficiently, we have to use the S2 star orbit data [93,94]. In particular, using solution (4), we can study the motion of the S2 star restricted in the equatorial plane ( $\theta = \pi/2, \dot{\theta} = 0$ ). From the Lagrangian it follows that

$$2\mathcal{L} = -f(r)\dot{t}^2 + \frac{\dot{r}^2}{f(r)} + r^2\dot{\phi}^2.$$

For the two constants of motion, namely total energy  $E$  and total angular momentum  $L$  of the star, we have  $\frac{\partial \mathcal{L}}{\partial \dot{t}} = -E$  and  $\frac{\partial \mathcal{L}}{\partial \dot{\phi}} = L$ . Using the above we find that

$$\dot{t} = \frac{E}{1 - \frac{(\Delta+2)M^{\Delta+1}(4\pi)^{\frac{\Delta}{2}}}{r}}, \tag{37}$$



along with  $\dot{\phi} = \frac{L}{r^2}$ . Finally, we have the following equation of motion for a massive particle (S2 star in our case) [97–99].

$$\ddot{r} = \frac{1}{2 g_{11}(r)} \left[ g_{00,r}(r) \dot{t}^2 + g_{11,r}(r) \dot{r}^2 + g_{33,r}(r) \dot{\phi}^2 \right]. \tag{38}$$

In general, one cannot find an analytical expression for  $r(\phi)$  and, therefore, one must elaborate numerically the equations of motion. In the present work we apply the Bayesian theorem with the likelihood function as given in [99,100], with the observational data for  $(X_{obs}, Y_{obs})$  given in [94,97], considering  $\Delta$  and  $M$  as free parameters. In order to find the best-fit values we use the Monte-Carlo-Markov Chains analysis. For the central mass object we take  $4.1 \times 10^6 M_{\odot}$  along with the uniform priors  $0 < \Delta < 1$  and  $0 < M < 2$ . In Figure 5 we present the region of the parameter space in agreement with S2 star data. Concerning Barrow parameter, in which we are interested in this manuscript, the best fit value and  $1\sigma$  errors are

$$\Delta \simeq 0.0036^{+0.0792}_{-0.0145}, \tag{39}$$

which is the main result of the present work.

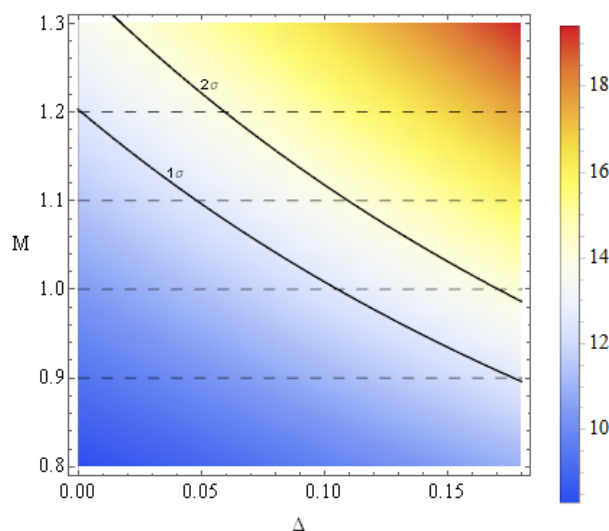


**Figure 4.** The predicted diameter per unit mass  $d$ , as a function of  $M$  and  $\Delta$ . The black curves correspond to the observationally determined upper  $1\sigma$  and  $2\sigma$  bounds given in (36) (the lower ones are not shown since they correspond to the not physically interested region  $\Delta < 0$ ).

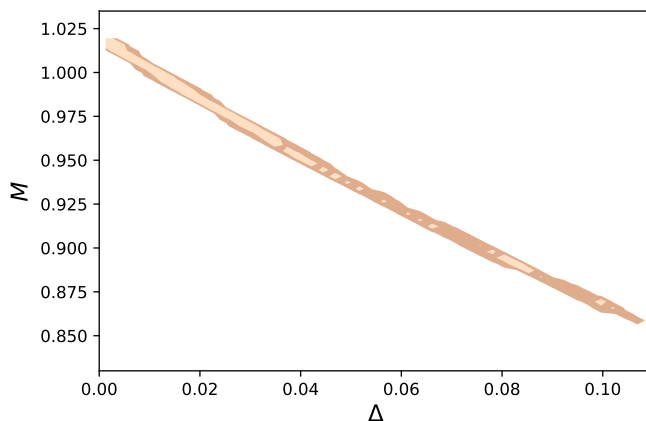


**Figure 5.**  $1\sigma$  and  $2\sigma$  parameter region consistent with S2 star observations, after a Monte-Carlo-Markov Chains analysis.

We can now combine the above result with the black hole shadow. In particular, applying the best-fit parameters we easily find the shadow radius  $R_{sh} = 5.3127$ , measured in units of black hole mass. Hence, in Figure 6 we depict the shadow image and intensity for a black hole with Barrow entropy, for the best-fit values of (39) and Figure 5.

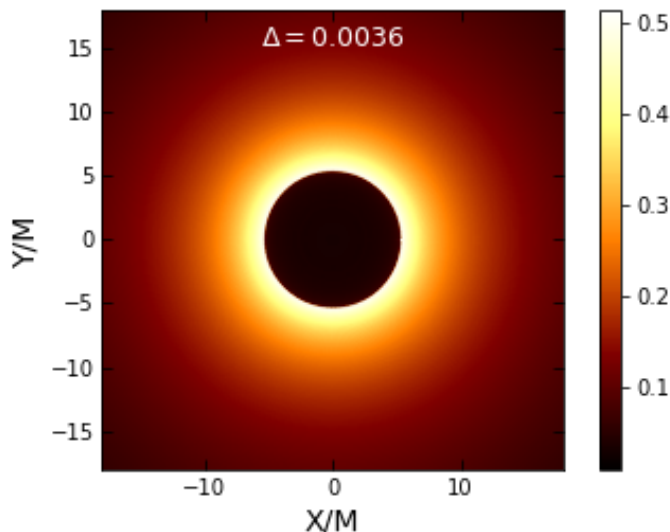


**Figure 6.** The shadow image and intensity for a black hole with Barrow entropy, for the best-fit values of (39) and Figure 5 arising from S2 star data with Monte-Carlo-Markov Chains analysis.

In summary, as we observe, although the standard value  $\Delta = 0$ , in which Barrow entropy becomes Bekenstein-Hawking entropy, lies inside the obtained  $1\sigma$  region, the best-fit value is  $\Delta = 0.0036$ , while the  $1\sigma$  upper bound is  $\Delta \lesssim 0.0828$ . Such constraint is stronger than the late-time cosmological ones from Supernovae (SNIa) Pantheon sample and cosmic chronometers (CC) datasets, namely  $\Delta \lesssim 0.188$  [101,102], but less strong than the Big Bang Nucleosynthesis (BBN) one, namely  $\Delta \lesssim 1.4 \times 10^{-4}$  [103], since the latter is known to lead to very strong constraints. Hence, it reveals the capabilities of black hole shadow and S2 star observations, since they can lead to significantly improved constraints although the data points are for the currently relatively few.

### 5. Conclusions

In this work we used data from M87\* central black hole shadow, as well as from the S2 star observations, in order to extract constraints on Barrow entropy. The latter is a modified entropy relation arising from quantum-gravitational effects that induce an intricate, fractal structure on the black hole horizon, quantified by the new Barrow parameter  $\Delta$ . Such a change in entropy leads to a change in temperature, as well as to the properties of the black hole and its shadow.

We investigated the photon sphere and the shadow of a black hole with Barrow entropy, and assuming a simple model for infalling and radiating gas we estimated the corresponding intensity. Furthermore, we used the radius in order to extract the real part of the quasinormal modes, and for completeness we investigated the spherical accretion of matter onto the black hole, focusing on isothermal and polytropic test fluids.

We used the EHT data from the M87\* black hole extracting the allowed parameter region, and then we additionally incorporated data from the motion of S2 star around the Sgr A\* black hole, through a Monte-Carlo-Markov Chains analysis, in order to break the degeneracies and extract the final constraints on the Barrow exponent. We found that  $\Delta \simeq 0.0036^{+0.0792}_{-0.0145}$  at  $1\sigma$  confidence level. Hence, our analysis places the upper bound  $\Delta \lesssim 0.0828$ , a constraint that is less strong than the Big Bang Nucleosynthesis (BBN) one, but significantly stronger than the late-time cosmological ones.

In summary, black-hole related data can serve as a new tool in order to test general relativity and examine if modifications of various kinds are allowed. Although the data points are currently few, they can be very efficient in constraining the theoretical parameters. The significant improvement of the datasets expected in the near future makes the corresponding analyses both interesting and necessary.

Although the M87\* is shown and expected to rotate, the Sgr A\* black hole might rotate very slowly compared to M87\*. In most applications pertaining to Sgr A\* rotation is dropped from consideration as in Refs. [98,99,104]. In that sense, the constraint we found for the S2 star is justified by assuming a nonrotating black hole in our galaxy. Rotation will be considered in a subsequent work.

**Author Contributions:** Writing—original draft, K.J., M.A.-A. and M.J.; Writing—review & editing, E.N.S. All authors have read and agreed to the published version of the manuscript.

**Funding:** This research received no external funding.

**Acknowledgments:** ENS would like to acknowledge the contribution of the COST Action CA18108 “Quantum Gravity Phenomenology in the multi-messenger approach”.

**Conflicts of Interest:** The authors declare no conflict of interest.

### Appendix A. Accretion of Matter onto Black Holes with Barrow Entropy

In this Appendix we investigate the accretion of matter onto black holes with Barrow entropy. We consider spherical accretion of a perfect fluid, whose stress-energy tensor is of the form  $T^{\mu\nu} = (e + p)u^\mu u^\nu + pg^{\mu\nu}$ , where  $e$  and  $p$  denotes the energy density and pressure, respectively. The black hole metric is assumed to be of the most general expression in spherical coordinates

$$ds^2 = -A(r)dt^2 + \frac{dr^2}{B(r)} + C(r)(d\theta^2 + \sin^2\theta d\phi^2). \tag{A1}$$

The particle and energy conservation during the accretion procedure are  $\nabla_\mu(nu^\mu) = 0$  and  $\nabla_\mu T^{\mu\nu} = 0$  respectively, where  $u^\mu = \frac{dx^\mu}{d\tau}$  is the four-velocity of the fluid particles ( $\tau$  is the proper time) and  $n$  is the particle density. Introducing the three-velocity as [105]  $v = \sqrt{\frac{1}{AB} \frac{u^r}{u^t}}$ , and using the steps developed in [106–111], we obtain the location  $r_c$  of the critical point (CP) and the value of the corresponding three-velocity as

$$v_c^2 = a_c^2 \quad \text{and} \quad (1 - a_c^2) \frac{A'}{A} \Big|_{r=r_c} = 2a_c^2 \frac{C'}{C} \Big|_{r=r_c}, \tag{A2}$$

where prime denotes derivative with respect to  $r$ ,  $v_c \equiv v|_{r=r_c}$ , and with  $a_c \equiv a|_{r=r_c}$  the three-dimensional speed of sound evaluated at the CP.

#### Appendix A.1. Isothermal Fluids

The equation of state of an isothermal fluid is of the form  $p = \omega e$  with  $0 < \omega < 1$  a constant. Since the sound speed  $a$  is defined by  $a^2 = dp/de$  we obtain  $a^2 = \omega$ , which depends of the particle’s position within the fluid. Since  $a$  is constant, the second equation of (A2) is easily solved knowing the metric (2) and (4), namely with  $A(r) = f(r)$  and  $C(r) = r^2$ , extracting the critical radius as

$$\tilde{r}_c = \left(3 + \frac{1}{a^2}\right) \frac{\tilde{r}_H}{4} = \left(3 + \frac{1}{a^2}\right) \frac{(4\pi)^{\frac{\Delta}{2}} (\Delta + 2) M^{\Delta+1}}{4}. \tag{A3}$$

Thus, for isothermal fluids a CP always exists since  $\tilde{r}_c > \tilde{r}_H$  for  $a^2 = \omega < 1$ . Hence, the isothermal fluid reaches the sound speed before it is absorbed by the black hole horizon.

When  $\omega = 1/3 = a^2$ , we have  $\tilde{r}_c = 3\tilde{r}_H/2$  which is the location of the photon sphere. This correspondence is discussed later on.

Appendix A.2. Polytropic Fluids

The polytropic equation of state is

$$p \propto n^\gamma, \quad (\gamma > 1). \tag{A4}$$

The corresponding sound speed takes the form [106,107]

$$a^2 = \frac{(\gamma - 1)\mathcal{X}}{m(\gamma - 1) + \mathcal{X}'}, \tag{A5}$$

where  $\mathcal{X} \propto n^{\gamma-1}$ , and with  $m$  the baryonic mass. Due to the particle conservation the number density  $n$  is a function of  $(r, v)$ , and thus  $a^2$  assumes the same dependence as  $n$ . This dependence was given in [106] leading to a complex relation between  $a^2$  and  $(r, v)$ , namely

$$a^2 = \frac{\mathcal{Y}(\gamma - 1)}{\left(\frac{1-v^2}{AC^2v^2}\right)^{\frac{1-\gamma}{2}} + \mathcal{Y}}, \tag{A6}$$

where  $\mathcal{Y} = \text{const.} > 0$  has dimensions of length to the power  $2(\gamma - 1)$ , and depends on  $(m, \gamma)$  and on the number density  $n_0$  at some initial point (e.g., the spatial infinity or the CP [106]). In this case the solution of the second equation in (A2) is still given by (A3), but with  $a^2$  replaced by  $a_c^2$  since  $a^2$  is no longer constant. Thus, reversing it we obtain

$$a_c^2 = \frac{\tilde{r}_H}{4\tilde{r}_c - 3\tilde{r}_H}. \tag{A7}$$

It is usually admitted that  $\gamma \leq 5/3$  and since (A6) implies  $a^2 < \gamma - 1 \leq 2/3$ , we see from (A3) that  $\tilde{r}_c > \tilde{r}_H$  and thus a CP always exists provided the r.h.s. of (A6) is positive and less than 1.

At the CP we have  $v_c^2 = a_c^2$  given by the r.h.s. of (A7). Substituting the above into (A6) we obtain the following transcendental equation for  $\tilde{r}_c$ :

$$\frac{\tilde{r}_H}{4\tilde{r}_c - 3\tilde{r}_H} = \frac{\mathcal{Y}(\gamma - 1)}{1 + \mathcal{Y}\left(\frac{4}{\tilde{r}_H\tilde{r}_c^3}\right)^{(\gamma-1)/2}} \left(\frac{4}{\tilde{r}_H\tilde{r}_c^3}\right)^{(\gamma-1)/2}. \tag{A8}$$

For the most used  $\gamma$  value in astrophysics, namely  $\gamma = 5/3$ , Equation (A8) can be solved explicitly as

$$\tilde{r}_c = \frac{9 \times 2^{2/3}\mathcal{Y}}{2^{11/3}\mathcal{Y} - 3\tilde{r}_H^{4/3}} \tilde{r}_H. \tag{A9}$$

To ensure that  $\tilde{r}_c > \tilde{r}_H$  and  $0 < a_c^2 < 1$  according to (A7) we require  $\mathcal{Y} > 3\tilde{r}_H^{4/3}/2^{11/3}$ . This provides a constraint between the parameters on which  $\mathcal{Y}$  depends and the parameters on which  $\tilde{r}_H$  depends. The sound speed at the PC is obtained inserting (A9) into (A7), namely

$$a_c^2 = \frac{2^{11/3}\mathcal{Y} - 3\tilde{r}_H^{4/3}}{3 \times 2^{8/3}\mathcal{Y} + 9\tilde{r}_H^{4/3}}, \tag{A10}$$

with  $\mathcal{Y} > 3\tilde{r}_H^{4/3}/2^{11/3}$ . Since  $\tilde{r}_H$  increases with  $\Delta$ , from (A9) we see that  $\tilde{r}_c$  increases too (respectively  $a_c^2$  decreases). Hence, as  $\Delta$  increases the CP occurs at advanced positions where the fluid particles acquire a lower critical speed  $v_c = a_c$ .

Appendix A.3. Correspondence: The Critical Point versus the Photon Sphere

In order to determine the photon sphere for the general metric (A1) we can repeat the steps of (12)–(22), finding that the radius of the photon sphere  $r_{ps}$  is determined by the equation [112,113]

$$\frac{A'}{A} \Big|_{r=r_{ps}} = \frac{C'}{C} \Big|_{r=r_{ps}}, \tag{A11}$$

which generalizes Equation (22). Comparing (A11) with the second equation in (A2) we see that the location of the CP would correspond to the radius of the photon sphere if

$$1 - a_c^2 = 2a_c^2 \Rightarrow a_c^2 = \frac{1}{3}. \tag{A12}$$

Since the sound speed  $a^2 = dp/de$  is position-dependent, Equation (A12) would be satisfied only if at the CP the value of  $a_c^2 = a^2|_{r=r_c}$  was just 1/3, which would mean that the CP occurs on the photon sphere.

There are special fluids where  $a^2$  is constant and we may consider the value 1/3. This is indeed the case for the isothermal radiation fluid with an equation of state of the form  $p = e/3$  resulting to  $a^2 \equiv 1/3$ . For such a fluid the CP always occurs on the photon sphere. However, for polytropic fluids, under specific conditions such a correspondence exists too. In particular, with  $a_c^2 = 1/3$  from (A7) we obtain  $\tilde{r}_c = 3\tilde{r}_H/2$ , and thus substituting into (A8) we extract the condition on  $\mathcal{Y}$  and  $\tilde{r}_H$ , namely

$$\tilde{r}_H^4 = \frac{32}{27} [(3\gamma - 4)\mathcal{Y}]^{2/(\gamma-1)}, \tag{A13}$$

alongside the previous condition (shown in (A10) for the case  $\gamma = 5/3$ ). Hence, for the case  $\gamma = 5/3$  this reduces to

$$\tilde{r}_H^{4/3} = \frac{2^{5/3}}{3} \mathcal{Y} < \frac{2^{11/3}}{3} \mathcal{Y}, \tag{A14}$$

which could be alternatively derived from (A10) setting  $a_c^2 = 1/3$ . Equation (A13) is a kind of fine-tuning condition between the parameters of the black hole, on the l.h.s., and the parameters of the polytropic fluid, on the r.h.s.

Hence, the sound speed at the critical point decreases with increasing  $\Delta$  and thus the location of the critical point advances away from the black hole. For both fluids we can see that the critical point may occur on the photon sphere under specific conditions. For isothermal fluids only the sound speed is constrained, while for polytropic fluids both the black hole and the fluid parameters are constrained.

References

1. Abbott, B.P. et al. [LIGO Scientific and Virgo Collaborations]. Observation of Gravitational Waves from a Binary Black Hole Merger. *Phys. Rev. Lett.* **2016**, *116*, 061102. [CrossRef]
2. Akiyama, K. et al. [Event Horizon Telescope]. First M87 Event Horizon Telescope Results. I. The Shadow of the Supermassive Black Hole. *Astrophys. J. Lett.* **2019**, *875*, L1.
3. Akiyama, K. et al. [Event Horizon Telescope]. First M87 Event Horizon Telescope Results. II. Array and Instrumentation. *Astrophys. J. Lett.* **2019**, *875*, L2.
4. Saridakis, E.N.; Lazkoz, R.; Salzano, V.; Moniz, P.V.; Capozziello, S.; Jiménez, J.B.; De Laurentis, M.; Olmo, G.J. Modified Gravity and Cosmology: An Update by the CANTATA Network. *arXiv* **2021**, arXiv:2105.12582.
5. Addazi, A.; Alvarez-Muniz, J.; Batista, R.A.; Amelino-Camelia, G.; Antonelli, V.; Arzano, M.; Asorey, M.; Atteia, J.L.; Bahamonde, S.; Bajardi, F.; et al. Quantum gravity phenomenology at the dawn of the multi-messenger era—A review. *arXiv* **2021**, arXiv:2111.05659.
6. Shaikh, R. Black hole shadow in a general rotating spacetime obtained through Newman-Janis algorithm. *Phys. Rev. D* **2019**, *100*, 024028. [CrossRef]
7. Wei, S.W.; Zou, Y.C.; Liu, Y.X.; Mann, R.B. Curvature radius and Kerr black hole shadow. *J. Cosmol. Astropart. Phys.* **2019**, *1908*, 030. [CrossRef]

8. Moffat, J.W.; Toth, V.T. Masses and shadows of the black holes Sagittarius A\* and M87\* in modified gravity. *Phys. Rev. D* **2020**, *101*, 024014. [[CrossRef](#)]
9. Firouzjaee, J.T.; Allahyari, A. Black hole shadow with a cosmological constant for cosmological observers. *Eur. Phys. J. C* **2019**, *79*, 930. [[CrossRef](#)]
10. Banerjee, I.; Mandal, B.; SenGupta, S. Does black hole continuum spectrum signal  $f(R)$  gravity in higher dimensions? *Phys. Rev. D* **2020**, *101*, 024013. [[CrossRef](#)]
11. Long, F.; Wang, J.; Chen, S.; Jing, J. Shadow of a rotating squashed Kaluza-Klein black hole. *J. High Energy Phys.* **2019**, *1910*, 269. [[CrossRef](#)]
12. Zhu, T.; Wu, Q.; Jamil, M.; Jusufi, K. Shadows and deflection angle of charged and slowly rotating black holes in Einstein-Æther theory. *Phys. Rev. D* **2019**, *100*, 044055. [[CrossRef](#)]
13. Konoplya, R.A.; Zhidenko, A. Analytical representation for metrics of scalarized Einstein-Maxwell black holes and their shadows. *Phys. Rev. D* **2019**, *100*, 044015. [[CrossRef](#)]
14. Contreras, E.; Rincón, Á.; Panotopoulos, G.; Bargeño, P.; Koch, B. Black hole shadow of a rotating scale-dependent black hole. *Phys. Rev. D* **2020**, *101*, 064053. [[CrossRef](#)]
15. Li, P.C.; Guo, M.; Chen, B. Shadow of a Spinning Black Hole in an Expanding Universe. *Phys. Rev. D* **2020**, *101*, 084041. [[CrossRef](#)]
16. Kumar, R.; Ghosh, S.G.; Wang, A. Gravitational deflection of light and shadow cast by rotating Kalb-Ramond black holes. *Phys. Rev. D* **2020**, *101*, 104001. [[CrossRef](#)]
17. Pantig, R.C.; Rodulfo, E.T. Rotating dirty black hole and its shadow. *Chin. J. Phys.* **2020**, *68*, 236. [[CrossRef](#)]
18. Xavier, S.V.M.C.B.; Cunha, P.V.P.; Crispino, L.C.B.; Herdeiro, C.A.R. Shadows of charged rotating black holes: Kerr–Newman versus Kerr–Sen. *Int. J. Mod. Phys. D* **2020**, *29*, 2041005. [[CrossRef](#)]
19. Guo, M.; Li, P.C. Innermost stable circular orbit and shadow of the 4D Einstein–Gauss–Bonnet black hole. *Eur. Phys. J. C* **2020**, *80*, 588. [[CrossRef](#)]
20. Roy, R.; Chakrabarti, S. Study on black hole shadows in asymptotically de Sitter spacetimes. *Phys. Rev. D* **2020**, *102*, 024059. [[CrossRef](#)]
21. Jin, X.H.; Gao, Y.X.; Liu, D.J. Strong gravitational lensing of a 4-dimensional Einstein–Gauss–Bonnet black hole in homogeneous plasma. *Int. J. Mod. Phys. D* **2020**, *29*, 2050065. [[CrossRef](#)]
22. Islam, S.U.; Kumar, R.; Ghosh, S.G. Gravitational lensing by black holes in the 4D Einstein-Gauss-Bonnet gravity. *J. Cosmol. Astropart. Phys.* **2020**, *2009*, 030. [[CrossRef](#)]
23. Chen, C.Y. Rotating black holes without  $\mathbb{Z}_2$  symmetry and their shadow images. *J. Cosmol. Astropart. Phys.* **2020**, *5*, 040. [[CrossRef](#)]
24. Konoplya, R.A.; Schee, J.; Ovchinnikov, D. Shadow of the magnetically and tidally deformed black hole. *arXiv* **2020**, arXiv:2008.04118.
25. Belhaj, A.; Benali, M.; Balali, A.E.; Hadri, W.E.; Moumni, H.E.; Torrente-Lujan, E. Black Hole Shadows in M-theory Scenarios. *arXiv* **2021**, arXiv:2008.09908.
26. Long, F.; Chen, S.; Wang, M.; Jing, J. Shadow of a disformal Kerr black hole in quadratic DHOST theories. *arXiv* **2020**, arXiv:2009.07508.
27. Contreras, E.; Rincón, Á.; Panotopoulos, G.; Bargeño, P. Geodesic analysis and black hole shadows on a general non-extremal rotating black hole in five-dimensional gauged supergravity. *arXiv* **2021**, arXiv:2010.03734.
28. Shao, W.H.; Chen, C.Y.; Chen, P. Generating Rotating Spacetime in Ricci-Based Gravity: Naked Singularity as a Black Hole Mimicker. *arXiv* **2021**, arXiv:2011.07763.
29. Ghosh, S.G.; Kumar, R.; Islam, S.U. Parameters estimation and strong gravitational lensing of nonsingular Kerr-Sen black holes. *arXiv* **2021**, arXiv:2011.08023.
30. Glampedakis, K.; Pappas, G. Can supermassive black hole shadows test the Kerr metric? *arXiv* **2021**, arXiv:2011.08023.
31. Konoplya, R.A.; Zhidenko, A. Shadows of parametrized axially symmetric black holes allowing for separation of variables. *Phys. Rev. D* **2021**, *103*, 104033. [[CrossRef](#)]
32. Wang, H.M.; Wei, S.W. Shadow cast by Kerr-like black hole in the presence of plasma in Einstein-bumblebee gravity. *arXiv* **2021**, arXiv:2106.14602.
33. Khodadi, M.; Lambiase, G.; Mota, D.F. No-hair theorem in the wake of Event Horizon Telescope. *J. Cosmol. Astropart. Phys.* **2021**, *09*, 028. [[CrossRef](#)]
34. Frion, E.; Giani, L.; Miranda, T. Black Hole Shadow Drift and Photon Ring Frequency Drift. *arXiv* **2021**, arXiv:2107.13536.
35. Zhu, Y.; Wang, T. Shadow of the wormhole-like static aether solution. *arXiv* **2021**, arXiv:2109.08463
36. Heydari-Fard, M.; Heydari-Fard, M.; Sepangi, H.R. On null geodesics and shadow of hairy black holes in Einstein-Maxwell-dilaton. *arXiv* **2021**, arXiv:2110.02713
37. Jusufi, K.; Saurabh. Black hole shadows in Verlinde’s emergent gravity. *Mon. Not. Roy. Astron. Soc.* **2021**, *503*, 1310. [[CrossRef](#)]
38. Davoudiasl, H.; Denton, P.B. Ultralight Boson Dark Matter and Event Horizon Telescope Observations of M87\*. *Phys. Rev. Lett.* **2019**, *123*, 021102. [[CrossRef](#)]
39. Bar, N.; Blum, K.; Lacroix, T.; Panci, P. Looking for ultralight dark matter near supermassive black holes. *J. Cosmol. Astropart. Phys.* **2019**, *1907*, 045. [[CrossRef](#)]
40. Jusufi, K.; Jamil, M.; Salucci, P.; Zhu, T.; Haroon, S. Black Hole Surrounded by a Dark Matter Halo in the M87 Galactic Center and its Identification with Shadow Images. *Phys. Rev. D* **2019**, *100*, 044012. [[CrossRef](#)]

41. Konoplya, R.A. Shadow of a black hole surrounded by dark matter. *Phys. Lett. B* **2019**, *795*, 1. [[CrossRef](#)]
42. Narang, A.; Mohanty, S.; Kumar, A. Test of Kerr-Sen metric with black hole observations. *arXiv* **2020**, arXiv:2002.12786.
43. Sau, S.; Banerjee, I.; SenGupta, S. Imprints of the Janis-Newman-Winicour spacetime on observations related to shadow and accretion. *Phys. Rev. D* **2020**, *102*, 064027. [[CrossRef](#)]
44. Belhaj, A.; Benali, M.; Balali, A.E.; Moumni, H.E.; Ennadifi, S.E. Deflection angle and shadow behaviors of quintessential black holes in arbitrary dimensions. *Class. Quant. Grav.* **2020**, *37*, 215004. [[CrossRef](#)]
45. Kumar, R.; Kumar, A.; Ghosh, S.G. Testing Rotating Regular Metrics as Candidates for Astrophysical Black Holes. *Astrophys. J.* **2020**, *896*, 89. [[CrossRef](#)]
46. Zeng, X.X.; Zhang, H.Q. Influence of quintessence dark energy on the shadow of black hole. *Eur. Phys. J. C* **2020**, *80*, 1058. [[CrossRef](#)]
47. Saurabh, K.; Jusufi, K. Imprints of dark matter on black hole shadows using spherical accretions. *Eur. Phys. J. C* **2021**, *81*, 490. [[CrossRef](#)]
48. Bambi, C.; Freese, K.; Vagnozzi, S.; Visinelli, L. Testing the rotational nature of the supermassive object M87\* from the circularity and size of its first image. *Phys. Rev. D* **2019**, *100*, 044057. [[CrossRef](#)]
49. Vagnozzi, S.; Visinelli, L. Hunting for extra dimensions in the shadow of M87\*. *Phys. Rev. D* **2019**, *100*, 024020. [[CrossRef](#)]
50. Haroon, S.; Jusufi, K.; Jamil, M. Shadow Images of a Rotating Dyonic Black Hole with a Global Monopole Surrounded by Perfect Fluid. *Universe* **2020**, *6*, 23. [[CrossRef](#)]
51. Shaikh, R.; Joshi, P.S. Can we distinguish black holes from naked singularities by the images of their accretion disks? *J. Cosmol. Astropart. Phys.* **2019**, *1910*, 064. [[CrossRef](#)]
52. Cunha, P.V.P.; Herdeiro, C.A.R.; Radu, E. EHT constraint on the ultralight scalar hair of the M87 supermassive black hole. *Universe* **2019**, *5*, 220. [[CrossRef](#)]
53. Banerjee, I.; Chakraborty, S.; SenGupta, S. Silhouette of M87\*: A New Window to Peek into the World of Hidden Dimensions. *Phys. Rev. D* **2020**, *101*, 041301. [[CrossRef](#)]
54. Feng, X.H.; Lu, H. On the size of rotating black holes. *Eur. Phys. J. C* **2020**, *80*, 551. [[CrossRef](#)]
55. Yan, S.F.; Li, C.; Xue, L.; Ren, X.; Cai, Y.F.; Easson, D.A.; Yuan, Y.F.; Zhao, H. Testing the equivalence principle via the shadow of black holes. *Phys. Rev. Res.* **2020**, *2*, 023164. [[CrossRef](#)]
56. Allahyari, A.; Khodadi, M.; Vagnozzi, S.; Mota, D.F. Magnetically charged black holes from non-linear electrodynamics and the Event Horizon Telescope. *J. Cosmol. Astropart. Phys.* **2020**, *2002*, 003. [[CrossRef](#)]
57. Rummel, M.; Burgess, C.P. Constraining Fundamental Physics with the Event Horizon Telescope. *J. Cosmol. Astropart. Phys.* **2020**, *2005*, 051. [[CrossRef](#)]
58. Vagnozzi, S.; Bambi, C.; Visinelli, L. Concerns regarding the use of black hole shadows as standard rulers. *Class. Quant. Grav.* **2020**, *37*, 087001. [[CrossRef](#)]
59. Khodadi, M.; Allahyari, A.; Vagnozzi, S.; Mota, D.F. Black holes with scalar hair in light of the Event Horizon Telescope. *J. Cosmol. Astropart. Phys.* **2020**, *2009*, 026. [[CrossRef](#)]
60. Chang, Z.; Zhu, Q.H. Does the shape of the shadow of a black hole depend on motional status of an observer? *Phys. Rev. D* **2020**, *102*, 044012. [[CrossRef](#)]
61. Kruglov, S.I. The shadow of M87\* black hole within rational nonlinear electrodynamics. *Mod. Phys. Lett. A* **2020**, *35*, 2050291. [[CrossRef](#)]
62. Ghosh, D.; Thalapillil, A.; Ullah, F. Astrophysical hints for magnetic black holes. *arXiv* **2020**, arXiv:2009.03363.
63. Psaltis, D. et al. [Event Horizon Telescope Collaboration]. Gravitational Test Beyond the First Post-Newtonian Order with the Shadow of the M87 Black Hole. *Phys. Rev. Lett.* **2020**, *125*, 141104. [[CrossRef](#)]
64. Hu, Z.; Zhong, Z.; Li, P.C.; Guo, M.; Chen, B. QED effect on a black hole shadow. *Phys. Rev. D* **2021**, *103*, 044057. [[CrossRef](#)]
65. Li, C.; Zhao, H.; Cai, Y.F. New test on the Einstein equivalence principle through the photon ring of black holes. *Phys. Rev. D* **2021**, *104*, 064027. [[CrossRef](#)]
66. Bekenstein, J.D. Black holes and entropy. *Phys. Rev. D* **1973**, *7*, 2333. [[CrossRef](#)]
67. Hawking, S.W. Particle Creation by Black Holes. *Commun. Math. Phys.* **1975**, *43*, 199. [[CrossRef](#)]
68. Barrow, J.D. The Area of a Rough Black Hole. *Phys. Lett. B* **2020**, *808*, 135643. [[CrossRef](#)]
69. Saridakis, E.N. Barrow holographic dark energy. *Phys. Rev. D* **2020**, *102*, 123525. [[CrossRef](#)]
70. Saridakis, E.N. Modified cosmology through spacetime thermodynamics and Barrow horizon entropy. *J. Cosmol. Astropart. Phys.* **2020**, *7*, 031. [[CrossRef](#)]
71. Mamon, A.A.; Paliathanasis, A.; Saha, S. Dynamics of an Interacting Barrow Holographic Dark Energy Model and its Thermodynamic Implications. *Eur. Phys. J. Plus* **2021**, *136*, 134. [[CrossRef](#)]
72. Huang, Q.; Huang, H.; Xu, B.; Tu, F.; Chen, J. Dynamical analysis and statefinder of Barrow holographic dark energy. *Eur. Phys. J. C* **2021**, *81*, 686. [[CrossRef](#)]
73. Rani, S.; Azhar, N. Braneworld Inspires Cosmological Implications of Barrow Holographic Dark Energy. *Universe* **2021**, *7*, 268. [[CrossRef](#)]
74. Adhikary, P.; Das, S.; Basilakos, S.; Saridakis, E.N. Barrow Holographic Dark Energy in non-flat Universe. *Phys. Rev. D* **2021**, *104*, 123519. [[CrossRef](#)]
75. Sheykhi, A. Barrow Entropy Corrections to Friedmann Equations. *Phys. Rev. D* **2021**, *103*, 123503. [[CrossRef](#)]

76. Abreu, E.M.C.; Neto, J.A. Some statistical approaches in the apparent horizon entropy and the generalized second law of thermodynamics. *arXiv* **2021**, arXiv:2107.04869.
77. Sharma, U.K.; Varshney, G.; Dubey, V.C. Barrow agegraphic dark energy. *Int. J. Mod. Phys. D* **2021**, *30*, 2150021. [[CrossRef](#)]
78. Lympferis, A.; Basilakos, S.; Saridakis, E.N. Modified cosmology through Kaniadakis horizon entropy. *Eur. Phys. J. C* **2021**, *81*, 1037. [[CrossRef](#)]
79. Drepanou, N.; Lympferis, A.; Saridakis, E.N.; Yesmakhanova, K. Kaniadakis holographic dark energy. *arXiv* **2021**, arXiv:2109.09181.
80. Telali, E.C.; Saridakis, E.N. Power-law holographic dark energy and cosmology. *arXiv* **2021**, arXiv:2109.09181.
81. Abreu, E.M.C.; Neto, J.A. Barrow black hole corrected-entropy model and Tsallis nonextensivity. *Phys. Lett. B* **2020**, *810*, 135805. [[CrossRef](#)]
82. Abreu, E.M.C.; Neto, J.A. Thermal features of Barrow corrected-entropy black hole formulation. *Eur. Phys. J. C* **2020**, *80*, 776. [[CrossRef](#)]
83. Abreu, E.M.C.; Neto, J.A.; Barboza, E.M., Jr. Barrow's black hole entropy and the equipartition theorem. *Europhys. Lett.* **2020**, *130*, 40005. [[CrossRef](#)]
84. Nojiri, S.; Odintsov, S.D.; Faraoni, V. Area-law versus Rényi and Tsallis black hole entropies. *arXiv* **2021**, arXiv:2109.05315.
85. Chandrasekhar, S. *The Mathematical Theory of Black Holes*; Oxford University Press: Oxford, UK, 2002.
86. Khodadi, M.; Saridakis, E.N. Einstein-Æther gravity in the light of event horizon telescope observations of M87\*. *Phys. Dark Univ.* **2021**, *32*, 100835. [[CrossRef](#)]
87. Jusufi, K. Quasinormal Modes of Black Holes Surrounded by Dark Matter and Their Connection with the Shadow Radius. *Phys. Rev. D* **2020**, *101*, 084055. [[CrossRef](#)]
88. Cuadros-Melgar, B.; Fontana, R.D.B.; de Oliveira, J. Analytical correspondence between shadow radius and black hole quasinormal frequencies. *Phys. Lett. B* **2020**, *811*, 135966. [[CrossRef](#)]
89. Narayan, R.; Johnson, M.D.; Gammie, C.F. The Shadow of a Spherically Accreting Black Hole. *Astrophys. J. Lett.* **2019**, *885*, L33. [[CrossRef](#)]
90. Zeng, X.X.; Zhang, H.Q.; Zhang, H. Shadows and photon spheres with spherical accretions in the four-dimensional Gauss-Bonnet black hole. *Eur. Phys. J. C* **2020**, *80*, 872. [[CrossRef](#)]
91. Falcke, H.; Melia, F.; Agol, E. Viewing the shadow of the black hole at the galactic center. *Astrophys. J. Lett.* **2000**, *528*, L13. [[CrossRef](#)]
92. Bambi, C. Can the supermassive objects at the centers of galaxies be traversable wormholes? The first test of strong gravity for mm/sub-mm very long baseline interferometry facilities. *Phys. Rev. D* **2013**, *87*, 107501. [[CrossRef](#)]
93. Gillessen, S.; Eisenhauer, F.; Fritz, T.K.; Bartko, H.; Dodds-Eden, K.; Pfuhl, O.; Ott, T.; Genzel, R. The orbit of the star S2 around SgrA\* from VLT and Keck data. *Astrophys. J. Lett.* **2009**, *707*, L114–L117. [[CrossRef](#)]
94. Abuter, R. et al. [GRAVITY Collaboration]. Detection of the gravitational redshift in the orbit of the star S2 near the Galactic centre massive black hole. *Astron. Astrophys.* **2018**, *615*, L15.
95. Walsh, J.L.; Barth, A.J.; Ho, L.C.; Sarzi, M. The M87 Black Hole Mass from Gas-dynamical Models of Space Telescope Imaging Spectrograph Observations. *Astrophys. J.* **2013**, *770*, 86. [[CrossRef](#)]
96. Shahzadi, M.; Kološ, M.; Stuchlík, Z.; Habib, Y. Testing alternative theories of gravity by fitting the hot-spot data of Sgr A\*. *arXiv* **2022**, arXiv:2201.04442.
97. Do, T.; Hees, A.; Ghez, A.; Martinez, G.D.; Chu, D.S.; Jia, S.; Sakai, S.; Lu, J.R.; Gautam, A.K.; O'Neil, K.K.; et al. Relativistic redshift of the star S0-2 orbiting the Galactic center supermassive black hole. *Science* **2019**, *365*, 664–668. [[CrossRef](#)] [[PubMed](#)]
98. Becerra-Vergara, E.A.; Arguëlles, C.R.; Krut, A.; Rueda, J.A.; Ruffini, R. Geodesic motion of S2 and G2 as a test of the fermionic dark matter nature of our Galactic core. *Astron. Astrophys.* **2020**, *641*, A34. [[CrossRef](#)]
99. Nampalliwar, S.; Kumar, S.; Jusufi, K.; Wu, Q.; Jamil, M.; Salucci, P. Modeling the Sgr A\* Black Hole Immersed in a Dark Matter Spike. *Astrophys. J.* **2021**, *916*, 116. [[CrossRef](#)]
100. Jusufi, K.; Kumar, S.; Azreg-Ainou, M.; Jamil, M.; Wu, Q.; Bambi, C. Constraining Wormhole Geometries using the Orbit of S2 Star and the Event Horizon Telescope. *arXiv* **2021**, arXiv:2106.08070.
101. Anagnostopoulos, F.K.; Basilakos, S.; Saridakis, E.N. Observational constraints on Barrow holographic dark energy. *Eur. Phys. J. C* **2020**, *80*, 826. [[CrossRef](#)]
102. Leon, G.; Na, J.M.; Hernández-Almada, A.; García-Aspeitia, M.A.; Verdugo, T.; Motta, V. Barrow Entropy Cosmology: An observational approach with a hint of stability analysis. *arXiv* **2021**, arXiv:2108.10998.
103. Barrow, J.D.; Basilakos, S.; Saridakis, E.N. Big Bang Nucleosynthesis constraints on Barrow entropy. *Phys. Lett. B* **2021**, *815*, 136134. [[CrossRef](#)]
104. Fragione, G.; Loeb, A. An upper limit on the spin of SgrA\* based on stellar orbits in its vicinity. *Astrophys. J. Lett.* **2020**, *901*, L32. [[CrossRef](#)]
105. Ellis, G.F.R.; Maartens, R.; MacCallum, M.A.H. *Relativistic Cosmology*; Cambridge University Press: Cambridge, UK, 2012.
106. Azreg-Ainou, M. Cyclic and heteroclinic flows near general static spherically symmetric black holes: Semi-cyclic flows—Addendum and corrigendum. *Eur. Phys. J. C* **2017**, *77*, 36. [[CrossRef](#)]
107. Ahmed, A.K.; Azreg-Ainou, M.; Faizal, M.; Jamil, M. Cyclic and heteroclinic flows near general static spherically symmetric black holes. *Eur. Phys. J. C* **2016**, *76*, 280. [[CrossRef](#)]



108. Azreg-Aïnou, M.; Ahmed, A.K.; Jamil, M. Spherical accretion by normal and phantom Einstein–Maxwell–dilaton black holes. *Class. Quant. Grav.* **2018**, *35*, 235001. [[CrossRef](#)]
109. Bahamonde, S.; Jamil, M. Accretion Processes for General Spherically Symmetric Compact Objects. *Eur. Phys. J. C* **2015**, *75*, 508. [[CrossRef](#)]
110. Ahmed, A.K.; Camci, U.; Jamil, M. Accretion on Reissner–Nordström–(anti)-de Sitter black hole with global monopole. *Class. Quant. Grav.* **2016**, *33*, 215012. [[CrossRef](#)]
111. Aslam, A.; Jamil, M.; Myrzakulov, R. Noether gauge symmetry for the Bianchi type I model in  $f(T)$  gravity. *Phys. Scr.* **2013**, *88*, 025003. [[CrossRef](#)]
112. Weinberg, S. Gravitation and Cosmology: Principles and Applications of the General Theory of Relativity. Available online: <https://www.amazon.com/Gravitation-Cosmology-Principles-Applications-Relativity/dp/0471925675> (accessed on 12 November 2021).
113. Kumar, R.; Islam, S.U.; Ghosh, S.G. Gravitational lensing by charged black hole in regularized 4D Einstein–Gauss–Bonnet gravity. *Eur. Phys. J. C* **2020**, *80*, 1128. [[CrossRef](#)]